6-1-2015

Ruling Out IC/CMB X-Rays In PKS 0637-752 And The Implications For TEV Emission From Large-Scale Quasar Jets

Eileen T. Meyer

Markos Georganopoulos

William B. Sparks

Leith E.H. Godfrey

James E.J. Lovell

See next page for additional authors

Authors

Eileen T. Meyer, Markos Georganopoulos, William B. Sparks, Leith E.H. Godfrey, James E.J. Lovell, and Eric S. Perlman

The Astrophysical Journal, 805:154 (8pp), 2015 June 1 doi:10.1088/0004-637X/805/2/154

RULING OUT IC/CMB X-RAYS IN PKS 0637-752 AND THE IMPLICATIONS FOR TEV EMISSION FROM LARGE-SCALE QUASAR JETS

Eileen T. Meyer[1,2], Markos Georganopoulos[2,3], William B. Sparks[4], Leith Godfrey[5], James E. J. Lovell[6], and Eric Perlman[7]
[1] Space Telescope Science Institute, Baltimore, MD 21218, USA; meyer@stsci.edu
[2] University of Maryland Baltimore County, Baltimore, MD 21250, USA
[3] NASA Goddard Space Flight Center, Greenbelt, MD 20771, USA
[4] Space Telescope Science Institute, Baltimore, MD 21218, USA
[5] ASTRON, Netherlands Institute for Radio Astronomy, P.O. Box 2, 7990 AA Dwingeloo, Netherlands
[6] School of Physical Sciences, University of Tasmania, Private Bag 37, Hobart, Tasmania 7001, Australia
[7] Florida Institute of Technology, Melbourne, FL 32901, USA
Received 2015 March 7; accepted 2015 April 2; published 2015 May 28

ABSTRACT

The *Chandra* X-ray observatory has discovered dozens of resolved, kiloparsec-scale jets associated with powerful quasars in which the X-ray fluxes are observed to be much higher than the expected level based on the radio-optical synchrotron spectrum. The most popular explanation for the anomalously high and hard X-ray fluxes is that these jets do not decelerate significantly by the kiloparsec scale, but rather remain highly relativistic (Lorentz factors $\Gamma \sim 10$). By adopting a small angle to the line of sight, the X-rays can thus be explained by inverse Compton upscattering of cosmic microwave background (CMB) photons (IC/CMB), where the observed emission is strongly Doppler boosted. Using over six years of *Fermi* monitoring data, we show that the expected hard, steady gamma-ray emission implied by the IC/CMB model is not seen in PKS 0637-752, the prototype jet for which this model was first proposed. IC/CMB emission is thus ruled out as the source of the X-rays, joining recent results for the jets in 3C 273 (using the same method) and PKS 1136-135 (using UV polarization). We further show that the *Fermi* observations give an upper limit of $\delta < 6.5$ for the four brightest X-ray knots of PKS 0637-752, and derive an updated limit of $\delta < 7.8$ for knots A and B1 of 3C 273 (assuming equipartition). Finally, we discuss the fact that high levels of synchrotron X-ray emission in a slow jet will unavoidably lead to a level of angle-integrated TeV emission which exceeds that of the TeV BL Lac class.

Key words: galaxies: active – galaxies: jets – quasars: individual (PKS 0637-752, 3C 273)

In 1999 August, the *Chandra* X-ray Observatory observed its first celestial target, quasar PKS 0637-752, during the initial focusing of the telescope (Chartas et al. 2000; Schwartz et al. 2000). Along with the bright quasar core, *Chandra* unexpectedly detected X-rays from the kiloparsec (kpc) scale relativistic jet (previously known from radio imaging, Figure 1). Unlike the synchrotron spectrum of lower-power FR I jets like M87 which easily extend up to X-ray energies (e.g., Wilson & Yang 2002), the synchrotron spectrum of powerful kpc-scale jets (including PKS 0637-752) generally peak at or below the IR/optical band. The X-rays detected in the kpc-scale jet of PKS 0637-752 were much brighter than expected from the radio-optical synchrotron spectrum, or indeed from either synchrotron self-Compton (SSC) or inverse Compton upscattering of ambient cosmic microwave background (CMB) photons (IC/CMB) assuming mildly relativistic kpc-scale flows under equipartition conditions (Chartas et al. 2000). Further, the X-ray spectrum of the jet was remarkably hard, with a photon index of 1.76 ± 0.1 (Figure 2).

Multi-epoch measurements of sub-parsec scale jets of powerful quasars with Very Long Baseline Interferometry (VLBI) have detected superluminal proper motions which imply that these jets start out highly relativistic, with Lorentz factors (Γ) of 10–50 (Jorstad et al. 2005; Lister et al. 2009). Though it had long been supposed based on population studies that jets decelerate and are at most mildly relativistic by the time they reach the kpc scale (e.g., Arshakian & Longair 2004; Mullin & Hardcastle 2009), no direct measurements have confirmed this. Tavecchio et al. (2000) and Celotti et al. (2001) thus suggested that the X-rays from the jet in PKS 0637-752 could be explained by IC/CMB emission if the jet *remained* highly relativistic ($\Gamma \sim 10$), and was pointed at a fairly small angle to our line of sight (6°). This produces a much larger Doppler boosting factor ($\delta \sim 10$) and enables the IC/CMB X-ray flux to match the observations.

Over the past decade and a half since the launch of *Chandra*, dozens more kpc-scale quasar jets with anomalously hard and/or high X-ray fluxes have been detected (e.g., Sambruna et al. 2001, 2002; Siemiginowska et al. 2003; Sambruna et al. 2004; Marshall et al. 2005; Harris & Krawczynski 2006; Siemiginowska et al. 2007; Marshall et al. 2011; Godfrey et al. 2012a; Kharb et al. 2012). The IC/CMB model has been by far the most popular explanation of these X-rays, though problems have been noted (e.g Hardcastle 2006; Harris & Krawczynski 2006). Besides the unconfirmed fast speeds required on the kpc scale, IC/CMB often requires the jet to be pointed very close along our line of sight (LOS), leading to a deprojected jet length longer than 1 Mpc, comparable to, or greater than the largest known giant radio galaxies (Dermer & Atoyan 2004). Further, the electrons responsible for upscattering the CMB into the *Chandra* band are at much lower energies than are traced by radio observations. This extension of the electron energy distribution is energetically costly, in some cases leading to "super-Eddington" jet power requirements (Dermer & Atoyan 2004; Uchiyama et al. 2006). Georganopoulos & Kazanas (2004) also noted that the commonly observed severe decrease in X-ray to radio flux ratio with distance down the jet (e.g., 3C 273, Jester et al. 2006) can only be reconciled with

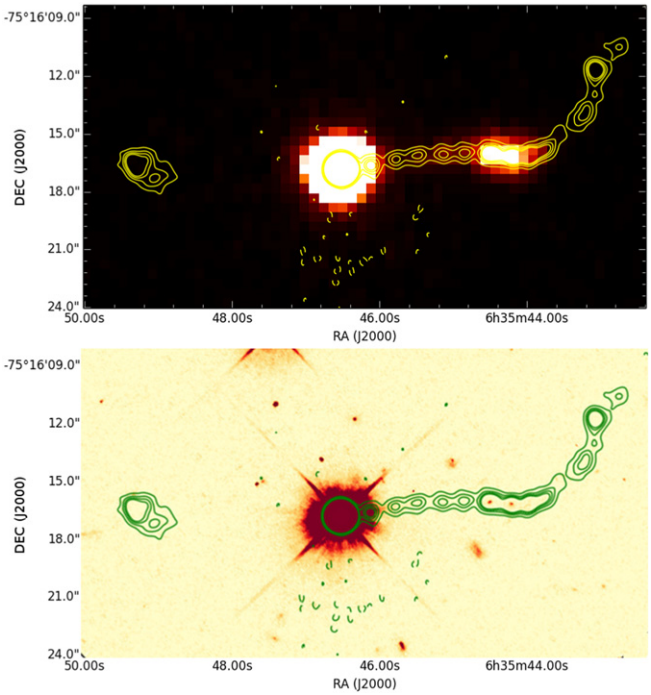

Figure 1. Upper panel: *Chandra* X-ray image of PKS 0637-752 (Chartas et al. 2000), with ATCA 18 GHz radio contours overlaid (Godfrey et al. 2012b). Lower panel: optical image of PKS 0637-752, taken with ACS/WFC on *HST* in F475W (Mehta et al. 2009) with ATCA 18 GHz radio contours overlaid.

IC/CMB X-rays if the jet is strongly decelerating. Hardcastle (2006), seeking to verify this for a sample of quasar jets, also noted that this explanation still leaves significant discrepancies with observations, namely the lack of similar deceleration profiles at kpc-scales for more misaligned jets. These problems lead to the suggestion that the X-rays could alternatively be synchrotron emission from a second electron population in the jet, albeit of unknown origin (Atoyan & Dermer 2004; Harris et al. 2004; Kataoka & Stawarz 2005; Hardcastle 2006; Jester et al. 2006; Uchiyama et al. 2006).

Despite a significant effort by the community to amass high-resolution radio, optical, and X-ray imaging of dozens of quasar jets, the fundamental problem up to now has been that fitting the radio-to-X-ray spectral energy distribution alone cannot distinguish between the IC/CMB and synchrotron explanations for the X-rays (Cara et al. 2013). The difference in power requirements between the two mechanisms is great, as is the extremely different idea of jet structure that they imply. Discriminating between these models is essential to make progress on the the physics of jets and their impact on their environments.

It was with an eye to resolving this long-standing deadlock that Georganopoulos et al. (2006), hereafter G06, suggested that *Fermi* Large Area Telescope (LAT) observations could confirm or rule out the IC/CMB mechanism for the X-rays, by detecting (or not) the high level of gamma-ray emission this mechanism predicts (Figure 2). We have previously looked for this gamma-ray emission from the jet of 3C 273, and ruled out IC/CMB gamma-rays from (the brightest) knot A alone at the >95% level, and from knots A through D1 combined at the >99.9% level (Meyer & Georganopoulos 2014, hereafter M14).

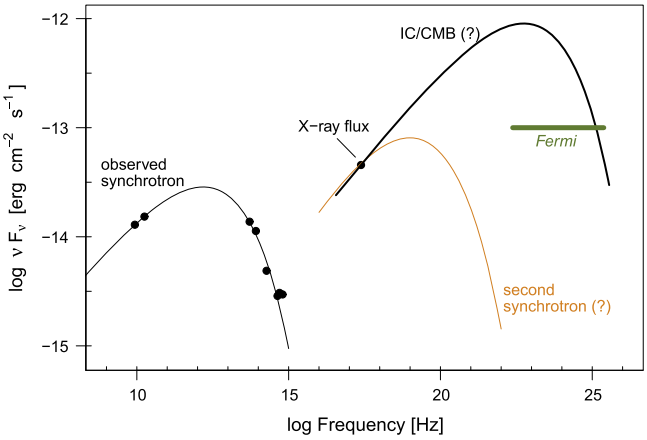

Figure 2. Depiction of the *Fermi* test for the X-ray emission mechanism in large-scale jets. Here we show the radio, optical, and X-ray photometry for the knots (total) in the jet of PKS 0637-752 as black points. The thin black line shows the synchrotron fit to the data. This synchrotron spectrum must be shifted by a factor 3.4×10^{10} in frequency and 3.05×10^{2} in luminosity, corresponding to $B/\delta = 1.5 \times 10^{-7}$ G, in order for the IC/CMB spectrum (thick black line) to match the X-ray flux level. As shown, this implies a high level of gamma-ray emission which should be detectable with *Fermi*. Alternatively, the X-rays could be due to a second synchrotron component (thin orange line).

In this paper we report new *Fermi* observations of PKS 0637-752 which show that the expected steady gamma-ray emission from the IC/CMB mechanism is also ruled out by deep upper limits at the 99.9% level. We also present updated limits for 3C 273, showing that the expected gamma-rays from IC/CMB are now ruled out at the 99.99% level in more than one *Fermi* energy band. We show that the deep upper limits at GeV energies place interesting constraints on the Doppler beaming factors which implies that these jets are not highly relativistic on the kpc scale. We further discuss the surprising implications of slow, synchrotron X-ray jets on our understanding of the total radiative output of quasars, especially at TeV energies.

1. METHODS

1.1. The Fermi Test of IC/CMB

As first noted by G06, the shape of the IC/CMB spectrum is constrained to match the synchrotron spectrum, with a shift in frequency and luminosity solely determined by the factor B/δ where δ is the Doppler beaming factor and B the magnetic field strength. From G06, we have:

$$\frac{\nu_c}{\nu_s} = \frac{\nu_{\rm CMB}\delta^2\gamma^2}{eB\delta\gamma^2/\left[2\pi m_e c(1+z)\right]} \quad (1)$$

$$\frac{L_c}{L_s} = \frac{32\pi U_{\rm CMB}(1+z)^4\delta^4}{3(B\delta)^2}, \quad (2)$$

where ν_c and ν_s (L_c, L_s) are the observed Compton and synchrotron frequencies (luminosities) emitted by electrons of Lorentz factor γ, e and m_e are the electron charge and mass, and $\nu_{\rm CMB} = 1.6 \times 10^{11}$ Hz is the CMB peak frequency at $z = 0$. However, if the observed X-ray fluxes are to be produced by the IC/CMB mechanism, then the value of B/δ is already uniquely determined by the requirement to match the X-ray flux level, at which point there is no freedom at all in the rest of

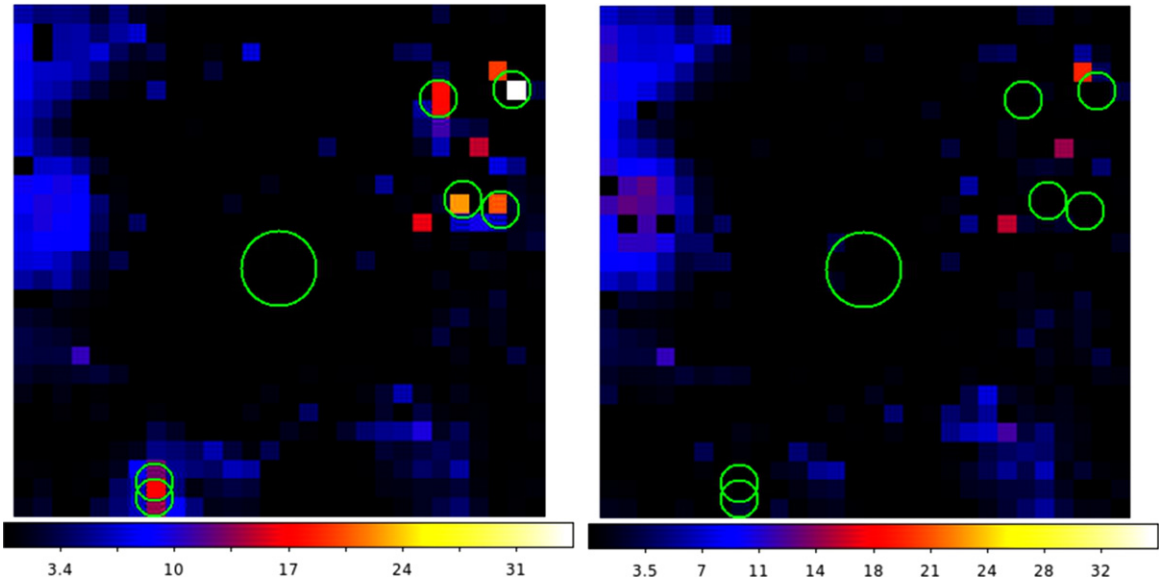

Figure 3. Left: an initial TS map of the region around PKS 0637-752, showing the excess TS present in 0.°5 pixels over the best-fit likelihood model using 2FGL catalog sources. The large circle marks the position of PKS 0637-752. The smaller circles mark the positions of the six new sources not present in the 2FGL catalog (corresponding to regions of excess TS with pixel values >20). Right: the updated TS map (same field of view and binning) after the six new sources were localized and fit with a binned likelihood.

the spectrum. The peak of the IC/CMB spectrum will fall in the GeV band, as shown in Figure 2. Note that this prediction is not predicated on any particular (e.g., equipartition) magnetic field strength.

The *Fermi*/LAT lacks the spatial resolution to detect the jet separately from the gamma-ray bright quasar core, which is only 10″ away—the *Fermi*/LAT 68% containment radius is on the order of tenths of a degree–degrees. However, in powerful quasars the inverse Compton core emission generally peaks at a few MeV, producing a soft and extremely variable spectrum in the *Fermi* band, with long periods of relative quiescence. Indeed, PKS 0637-752 was detected in the 2nd *Fermi* source catalog (2FGL, Nolan et al. 2012) as source 2FGL J0635.5-7516, with a very soft spectrum (photon index of $\Gamma_p = 2.71$) and high degree of variability (variability index = 347). In contrast, the IC/CMB emission from the large scale jet is expected to be harder and completely non-variable. The latter property allows us to combine the *Fermi* data taken only when the quasar core is in a low state to try to detect or place limits on the IC/CMB emission.

1.2. Fermi Analysis of PKS 0637-752

We first combined the all-sky weekly LAT event and spacecraft files for weeks 9 through 325 of the *Fermi* mission, corresponding to *Fermi* Mission Elapsed Time from 239557417 to 430608212 and calendar dates 2008 August 4 to 2014 August 24. In order to analyze the region around PKS 0637-752, we used the publicly available "quickAnalysis" script[9] to run the *Fermi* analysis tools and generate the filtered event file, livetime cube, and exposure map, using a region of interest (ROI) of 10° and an otherwise default configuration. The starting source list was generated from the publicly available `make2FGLxml` script, which generates the xml file pre-populated with 2FGL catalog sources. We used a binned maximum likelihood to get an initial fit for all the catalog sources in our ROI. We also included sources a further 5° out from our ROI, but with spectral parameters fixed to the 2FGL catalog values. PKS 0637-752 was detected with a very high test-statistic (TS, roughly significance squared) value of 289, a 100 MeV to 100 GeV photon flux of 3.16×10^{-8} s^{-1} cm^{-2}, and a photon index $\Gamma_p = 2.64$, similar to the value reported in the 2FGL catalog.

We checked for additional significant sources within 7° of PKS 0637-752 but not in the two year LAT catalog by making a TS residual map. The TS map was created by first freezing all source parameters in the initial model to their best-fit values, and then checking what TS value a test point source at different locations would be given. The resulting initial TS map is shown at left in Figure 3. In two areas the coarse 0.°5 binning did not allow separation of what appeared to be multiple components, and so a finer 0.°125 binning was used over these smaller areas to determine the rough location of new sources.

Rough starting positions of apparent new significant sources were measured from the TS map by hand, only considering as candidates those with a central pixel value (TS) >20. Each potential new source was then localized one at a time as follows. A power-law point source was added at the rough location of the excess TS, with normalization and powerlaw index free. Sources within 5° of the new source also had normalization/index parameters free. We ran a binned likelihood to get a starting fit for the new source plus other sources in the area. The fit parameters were then frozen again, so that we could next optimize the R.A./decl. location of the new source. The existing tool, `gtfindsrc`, only works for unbinned likelihood analysis, so we built our own binned version of the tool which works in the same way. Using the frozen model, we used the python `minimize` function in the `scipy` package (L-BFGS-B method) to optimize the log-likelihood value versus the R.A. and decl. position, given a reasonable range of about 1° around the starting positions noted by hand. We then update our new source in the model with this

[9] The public scripts mentioned in the text are available at http://fermi.gsfc.nasa.gov/ssc/data/analysis/user/.

Table 1
New Sources in ROI of Targets

Near PKS 0637-752			Near 3C 273		
R.A.	decl.	TS	R.A.	decl.	TS
82.43046	−72.74572	57.5	192.82676	−2.00263	70.7
81.13040	−69.60575	60.5	190.96827	−2.29561	82.3
78.98804	−72.72570	28.6	187.15935	−3.29476	60.2
86.33797	−70.34640	39.6	184.47577	−0.48239	92.5
119.70430	−80.70430	9.9	193.43690	3.47391	224.6
118.83300	−80.32970	16.1	192.63313	2.25116	65.7

Note. R.A. and decl. are in J2000 epoch.

optimized position (positions always remain fixed when optimizing over spectral parameters). We un-freeze the normalization and index of the new source and the local sources and run a final binned likelihood optimization to get an updated model of all sources in the ROI. This is then the starting model for the next new source to be added, until all new sources have been localized and a final optimized fit derived. For the 7° ROI around PKS 0637-752, six new sources were added to the model, and an updated TS map run from this larger source list shows that the excess TS previously seen is now gone (right panel of Figure 3). A list of the new sources with their location and TS value is given at left in Table 1.

As the PKS 0637-752 core is a significant *Fermi* source, our approach to detecting and/or setting limits on the IC/CMB gamma-ray emission exploits the variability of the core which cannot be spatially resolved separately from the large-scale jet due to the poor angular resolution of *Fermi*. During times when the blazar is quiescent, the hard, steady emission from IC/CMB will either appear as a steady plateau, or else the upper limits generated will place constraints on the level of the IC/CMB emission.

In order to build a light curve of the core, the full six year dataset was divided into bins of equal good time interval (GTI) time, totaling 10.5 days. We then used our updated (2FGL + 6 new) model described above and ran a binned likelihood to fit PKS 0637-752 as a power-law source, with sources more than 5° away fixed. The resulting light curve for the core over the full time range is shown in Figure 4, with the 100 MeV–100 GeV photon flux shown on top and the corresponding TS shown below. The clear variability in the light curve indicates that the total *Fermi* flux is dominated by the core.

We next began a "progressive binning" analysis, in which the light curve bins were ordered from lowest to highest TS value. Of the entire set of 75 time bins, 27 showed a TS level consistent with zero for the location of PKS 0637-752 (upper limits in lower panel of Figure 4). Starting from these 27 bins combined, we progressively combine the event files for the lowest bins plus the next lowest bin in TS, at each step optimizing the fit of PKS 0637-752 and the sources within 5° with a binned likelihood. We repeated adding the next-highest bin and getting the maximum likelihood fit until all bins had been added together. Note that this re-combining of the light curve in a discontinuous way is appropriate for deriving a limit on the large-scale jet because the IC/CMB emission is predicted to be completely non-variable, and thus there is no risk of any selection effect via variability. The variable core clearly dominates the flux levels determining the ordering, and is disconnected from the jet in any case. At each step we evaluated the TS and flux level in the five canonical *Fermi*

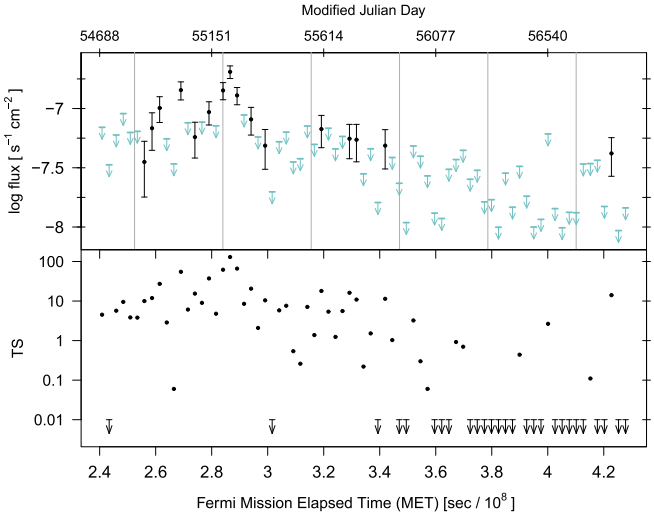

Figure 4. Upper: light curve of PKS 0637-752. The total 100 MeV–100 GeV photon flux for PKS 0637-752 in 10.5 day (total GTI) bins vs. the mean Mission Elapsed Time (MET) of the bin. Upper limits are shown where TS < 10. The gray vertical lines correspond to the start of a calendar year, beginning with 2009. Lower: the TS value of the bin vs. MET.

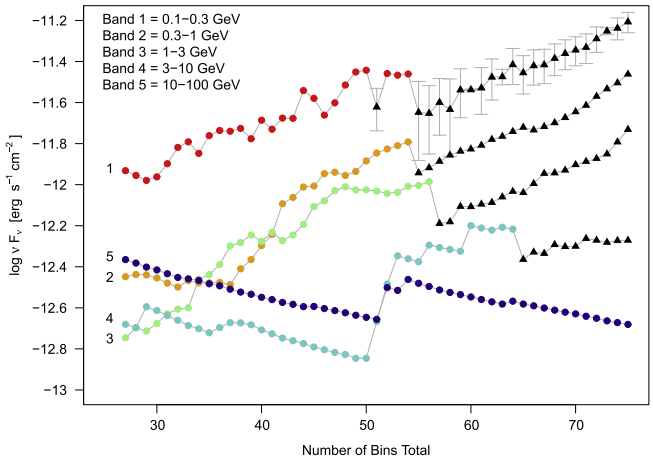

Figure 5. Results of the progressive binning analysis on PKS 0637-752. The upper axis gives the νF_ν flux while lower axis gives the total number of bins combined (where ordering is based on TS value and not time order), starting from the 27 bins with TS < 0.01. The points give the upper limits (colored dots) or detected fluxes (TS > 10, black triangles) for each of the five *Fermi* energy bands (red, orange, green, cyan, navy from lowest to highest energy). Errors on the detected fluxes are only shown for the lowest-energy band for clarity but are similar across bands. For the highest-energy band (10–100 GeV) no detection is ever made. The increasing detected fluxes indicate that the quasar core is being detected in the other bands.

energy bands of 0.1–0.3, 0.3–1, 1–3, 3–10, and 10–100 GeV, calculating the 95% upper limit flux value when TS < 10 in any given bin. Previous work on 3C 273 has shown that the exact method of ordering the bins (whether by using the TS value or the total flux or upper limit value for the bin) does not significantly affect the order or resulting upper limits (M14).

As shown in Figure 5, the highest energy bands gave upper limits which decreased with the increasing exposure as more bins are added, where we have color-coded the upper limits in the five energy bands, and black triangles indicate a significant detection in the band. Note that in the lower-energy bins, where the PKS 0637-752 quasar core dominates due to its soft spectrum, the upper limits reach a minimum rather quickly, and generally increase before becoming detections. It must be noted

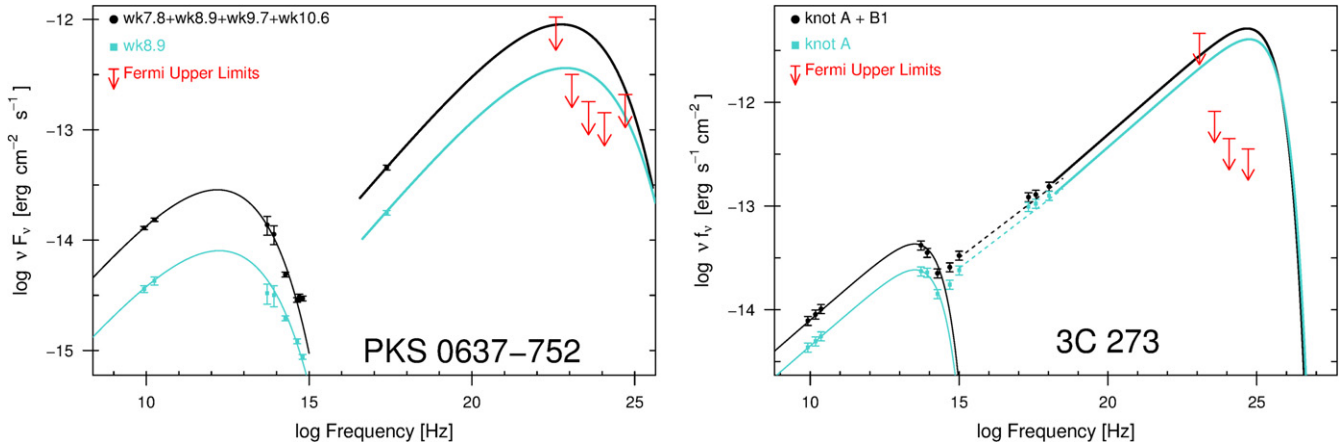

Figure 6. Left: the SED for the large-scale jet of PKS 0637-752. Data for the four brightest X-ray detected knots combined is shown as black points. The SED of the X-ray brightest knot, wk8.9, is plotted with blue points. Right: the SED for the knots of 3C 273, with black points for knots A and B1 combined, and blue for X-ray brightest knot A only. For both plots, the *Fermi* 95% upper limits are shown in red.

that the detected gamma-ray emission in these bands is from the quasar core, not the large-scale jet, based on the soft spectrum, and the fact that the emission level rises as more bins are added (showing that the source is indeed variable and that the bins are ordered by flux level). If we were to detect the large-scale jet, we would expect it to contribute significantly in the two highest-energy *Fermi* bands, and also to remain steady in flux level after the exposure became long enough to detect it. This latter point is important for distinguishing a detection of IC/CMB gamma-rays versus the tail of the Compton emission from the core, which should (like the low-energy bins) rise in flux as more bins are added. While the fourth energy band detected points do not rise as quickly as the first three, the flux level is far above the upper limit derived after 50 bins, so cannot be the steady emission of the large-scale jet, which must be below this limit. The highest bin never shows a significant detection of either component.

1.3. Fermi Analysis of 3C 273

We re-analyzed the *Fermi* data for 3C 273 using the 6 year dataset to compare with the results from M14 using 4.5 years of data, as the core remained relatively quiescent over the additional time elapsed. We followed the same procedure as outlined above for PKS 0637-752, finding six new sources within 7° of the position of 3C 273, listed at right in Table 1. The core of 3C 273 was detected with a TS of 17504, with a 100 MeV–100 GeV photon flux of 3.68×10^{-7} s^{-1} cm^{-2} and $\Gamma_p = 2.67$. A light curve was made using bins totaling 10.5 days in GTI time, and ordered according to TS (a total of 88 bins). The progressive-binning was started from the single lowest bin, with the next-highest bin continually added as described above until all bins were added. At each step the flux (or 95% upper limit) was calculated for the five canonical *Fermi* energy bins, as for PKS 0637-752.

2. RESULTS: TESTING THE IC/CMB MODEL

We show in Figure 6 the radio to X-ray SEDs for the jet of both PKS 0637-752 (left) and 3C 273 (right). For PKS 0637-752 we have taken both the *Chandra* X-ray and *Hubble Space Telescope* (*HST*) infrared and optical data (NICMOS, WFPC2 and ACS) from Mehta et al. (2009). We have also re-derived the *Spitzer* infrared fluxes for the brightest complex of knots (wk7.8, wk8.9, wk9.7, wk10.7), following the same methods reported in Uchiyama et al. (2005). We have also measured updated radio fluxes based on a re-analysis of archival and new ATCA data at 4.8, 8.4, and 17.8 GHz (first published in Godfrey et al. 2012b). For 3C 273, data is taken from Jester et al. (2005, 2006) and Uchiyama et al. (2006) and references therein.

In both figures, we consider two scenarios: the first combines the photometry of the brightest/nearest knots to the core in order to test the IC/CMB prediction (black points and lines). In 3C 273, Jester et al. (2005) have already shown that only knots A and B1 have X-ray indices similar to their radio indices (which is required for IC/CMB), so our "combined knot" scenario includes only these two knots. For PKS 0637-752, we use all the bright X-ray knots just before the turn in the jet (wk7.8, wk8.9, wk9.7, and wk10.6) where one might assume that some deceleration likely takes place. We do not include the only other X-ray detected knot (wk5.7) because it is not consistently detected at other wavelengths. The second scenario assumes that the X-rays from the weaker knots are already *not* from IC/CMB, and so only the photometry of the X-ray brightest knot is plotted: knot A in 3C 273 and wk8.9 in PKS 0637-752, in both cases plotted as blue points and lines. The thin solid lines through radio-optical points show a (phenomenological) synchrotron spectrum fitting the data, while the heavy line shows the corresponding IC/CMB curve to match the X-ray flux levels. As shown, for both jets, the 95% upper limits in several bands violate the IC/CMB predictions under either scenario.

We report in Table 2 a summary of the *Fermi* data analysis for PKS 0637-752 and 3C 273. We list the definition of the energy bins in columns 2–5, followed by the deepest 95% upper limit flux level (in νF_ν) reached in our progressive binning for each energy bin in column 6. The corresponding number of bins co-added to reach that limit is given in column 7. In column 8 we list the flux predicted under the IC/CMB at the frequency given in column 5. This flux corresponds to the IC/CMB model prediction for the combination of knots wk7.8, wk8.9, wk9.7, and wk10.7 in PKS 0637-752, and knots A and B1 for 3C 273. In column 10, we have calculated at what significance level our observations rule out the level of predicted IC/CMB flux given in column 9. For the final two columns, we also give the predicted flux under IC/CMB and

Table 2
Results of the Fermi Data Analysis

Source	Band	E_1 (GeV)	E_2 (GeV)	log Frequation (Hz)	95% upper Limit (erg s^{-1} cm^{-2})	Bins Added	Combined Knots[a]		Single Knot[b]	
							$F_{IC/CMB}$ (erg s^{-1} cm^{-2})	% Ruled Out	$F_{IC/CMB}$ (erg s^{-1} cm^{-2})	% Ruled Out
(1)	(2)	(3)	(4)	(5)	(6)	(7)	(8)	(9)	(10)	(11)
0637-752	1	0.1	0.3	22.6	1.05×10^{-12}	29	9.0×10^{-13}	92.9	3.6×10^{-13}	…
	2	0.3	1	23.1	3.17×10^{-13}	32	8.8×10^{-13}	99.8	3.6×10^{-13}	94.5
	3	1	3	23.6	1.80×10^{-13}	27	7.4×10^{-13}	99.98	3.2×10^{-13}	98.7
	4	3	10	24.1	1.43×10^{-13}	50	5.3×10^{-13}	99.95	2.5×10^{-13}	98.6
	5	10	100	24.7	2.09×10^{-13}	75	2.3×10^{-13}	95.9	1.3×10^{-13}	…
3C 273	1	0.1	0.3	22.6	2.72×10^{-11}	1	2.1×10^{-12}	…	1.6×10^{-12}	…
	2	0.3	1	23.1	4.63×10^{-12}	2	2.8×10^{-12}	…	2.1×10^{-12}	…
	3	1	3	23.6	8.20×10^{-13}	5	3.6×10^{-12}	>99.99	2.8×10^{-12}	>99.99
	4	3	10	24.1	4.46×10^{-13}	31	4.5×10^{-12}	>99.99	3.5×10^{-12}	>99.99
	5	10	100	24.7	3.56×10^{-13}	30	5.2×10^{-12}	>99.99	4.1×10^{-12}	>99.99

[a] Combined Knots are wk7.8, wk8.9, wk9.7, and wk10.6 for PKS 0637-752, knots A and B1 for 3C 273.
[b] Single Knots are wk8.9 for PKS 0637-752 and knot A for 3C 273.

the significance-level that we can rule it out, but only for the X-ray brightest knot of each jet (wk8.9 and knot A, respectively). As shown, the IC/CMB model is ruled out at a >99.9% level for PKS 0637-752 and at >99.99% level for 3C 273 under the combined knot scenarios, and ruled out at the 98.7% level for PKS 0637-752 and at >99.99% level for 3C 273 when considering only the single brightest knot.

3. DISCUSSION

These two cases where the IC/CMB origin for the X-rays has been unambiguously ruled out join with that of PKS 1136-135, where high UV polarization has shown that the second component (UV to X-ray) must be synchrotron in origin, since significant polarization is not expected in the IC/CMB scenario (Cara et al. 2013). The UV polarization method is unfortunately not able to be applied in general, as not all of the known quasar jets show the second component already dominating in the UV, being instead dominated by the radio-optical synchrotron component, though we note that 3C 273 could be confirmed in this way.

With IC/CMB ruled out in these three cases, we must explore alternative sources of X-ray emission for these knots. SSC emission was ruled out very early on as being far too weak (Chartas et al. 2000), unless very low (far from equipartition) magnetic fields were adopted; however, the total power requirement then becomes far too high ($>10^{49}$ erg s^{-1}) and the Doppler factor very small ($\ll 1$) suggesting an unrealistically de-beamed jet (Tavecchio et al. 2000; Dermer & Atoyan 2004). A viable alternative, though requiring further exploration, is a hadronic origin for the X-rays. Such models (e.g., Aharonian 2002) would not be in conflict with the high polarization measurements of Cara et al. (2013), and these models may be tunable enough to match the X-ray flux level while avoiding the GeV limits (Zhang and Böttcher 2013; Kundu & Gupta 2014). A (leptonic) synchrotron origin for the X-rays from a second population of electrons is also not in conflict with any of the data in hand, and further, relaxes many of the "uncomfortable" constraints of the IC/CMB model. Very small angles to the line of sight are not required, and the total jet power required is considerably less (Dermer & Atoyan 2004), as the electron energy distribution need not be extended to very low values. The main objection to a second synchrotron component heretofore has simply been its unexplained nature; Schwartz et al. (2000) notes that there is no reason why a second population of high-energy electrons should be co-spatial with the first. However, this co-occurrence of two very different electron populations, if the correct interpretation, is obviously a very important clue to the particle acceleration mechanism in large-scale jets, of which we still know little. An additional characteristic of the second electron population, at least for the case of PKS 0637-752, is that it requires a low-energy-cutoff in the electron energy distribution at TeV energies, otherwise the spectrum should extend to optical energies, contrary to the cutoff seen in the radio optical knot emission (Mehta et al. 2009). Acknowledging that further work may be warranted in the direction of evaluating hadronic models, we focus the rest of the paper on the implications for jet physics if the X-ray flux in quasar jets is synchrotron emission from a separate, high-energy electron population.

Assuming that the X-ray emission from the jets of 3C 273 and PKS 0637-752 is synchrotron in origin, an interesting consequence follows for our accounting of the large-scale-jet contribution to various backgrounds, especially at TeV energies. Jet one-sidedness clearly indicates that the kpc-scale jets are at least mildly relativistic, and thus IC/CMB emission must occur at some level. Due to the very low background in the highest-energy *Fermi* bands, the flux limits reachable by *Fermi*'s sky-scanning mode of operation should allow us to eventually either detect this emission or put very strong limits on the factor of B/δ which characterizes the flow on the kpc scale. The current *Fermi* 95% upper limits already constrain $\delta \lesssim 7.8$ for 3C 273 and $\delta \lesssim 6.5$ PKS 0637-752, under the assumption of equipartition magnetic fields, where we take $B\delta = 1.5 \times 10^{-5}$ G for PKS 0637-752 from Tavecchio et al. (2000) and $B\delta = 1.0 \times 10^{-4}$ for 3C 273 from Jester et al. (2006). Lower magnetic field values would only decrease these upper limits on δ. These limits are already low enough to have interesting consequences for our understanding of the total radiative output of AGN jets on the kpc scale.

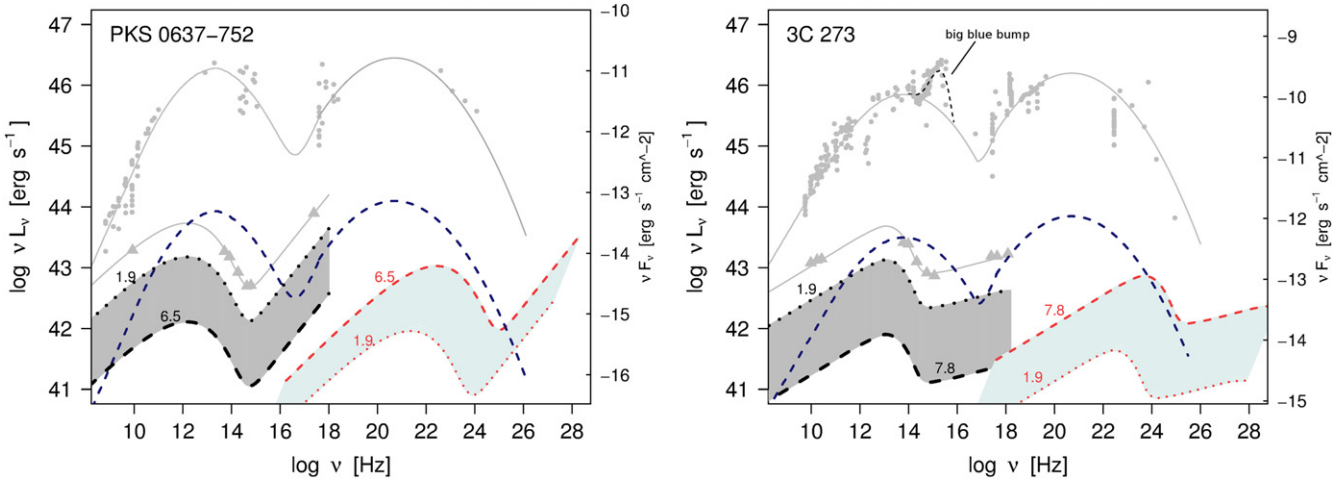

Figure 7. Note: figure description below applies to both panels; PKS 0637-752 is shown at left and 3C 273 is shown at right. The core flux points are shown as gray circles with phenomenological SED fit through the points drawn as a thin gray line. The big blue bump, visible only in 3C 373, is shown as black dashed line and not included in the beamed emission fits. In comparison, the total kpc-scale jet flux shown as gray triangles. The flux scale at right only applies to solid curves in the figure. The impression of the total dominance of the core flux is mainly a product of the beaming difference between the two components, as seen when beaming-corrected (angle-integrated) luminosities are plotted, rather than those assuming isotropy. Blue dashed line is the core fit times $1/\delta^2$ with $\delta = 15$ for both jets, representing the angle-integrated total core output. The gray zone is the range of possible angle-integrated output for the knots given our current constraints on δ for the knots. Finally, the light blue shaded area is the range of IC/CMB emission from the knots possible given the same δ constraints. Note that the TeV emission in particular is already constrained to be much higher than is typical for TeV blazars ($\approx 10^{41}$ erg s^{-1}).

It is generally assumed that the radiative output of quasar jets is dominated by that occurring at the "core," the base of the jet which is presumed to be very near the black hole (or $\sim$ parsecs away at most) and is therefore unresolved even in VLBI imaging. Certainly, the observed fluxes are dominated by this part of the jet due to Doppler beaming whenever the jet is pointed fairly along our LOS. This is depicted in Figure 7, where the core flux of both jets are shown as gray circles, and the total kpc-scale jet as gray triangles (flux scale on right axis). The luminosity scale at left applies to these points only under the incorrect assumption of isotropy. If we correct these values for beaming, we get the real "angle-integrated" total power output from the core and the jet, plotted as a dark blue dashed line and the gray shaded area, respectively. VLBI observations of superluminal motions place a lower limit on $\Gamma = 15$ for the cores of both 3C 273 and PKS 0637-752, respectively (Edwards et al. 2006; Lister et al. 2013). We have applied a correction (multiplying by $1/\delta^2$, Ghisellini & Tavecchio 2010) assuming $\delta = 15$ for the cores of both jets to give the angle-integrated core luminosity (dark blue dashed line). To calculate the angle-integrated luminosity of the knots, we apply a lower limit value of $\delta = 1.9$ which comes from statistical arguments based on populations (Arshakian & Longair 2004), which gives the dotted-line upper edge to the gray shaded area, while the current δ limits from *Fermi* give the lower dashed-line limit. The true angle-integrated luminosity of the knots is thus somewhere in the gray zone.

Comparing the dashed-blue curve and the gray shaded area, it is interesting to note that the knots are apparently *not* necessarily insignificant in total output when compared to the core. The jet power dissipated by radiative losses appears to occur over much larger physical scales than has previously been appreciated. Definite conclusions will require tighter constraints on the δ factors of both the core and the knots, but it is possible that large-scale jets contribute more than the core in the UV to X-rays, in addition to their general dominance in the radio. Large-scale jets could thus also be a contributor to some astrophysical backgrounds.

A further observation follows from the realization that the X-rays are synchrotron in origin: the electrons producing the synchrotron X-rays will themselves upscatter the CMB to produce a GeV to TeV spectrum. The angle-integrated total power in the IC/CMB component is shown in Figure 7 as a light blue shaded area. Note that the bounds in this case are flipped; the upper δ limit forms the upper edge of the allowed zone. This is because IC/CMB emission increases with the Doppler factor as δ^2 even after the angle-integrated 4π luminosity correction is included. Even in the minimum $\delta = 1.9$ case, these jets are already constrained to produce fluxes in excess of 10^{41} erg s^{-1} which is the typical angle-integrated luminosity for canonical TeV blazars (adopting an observed luminosity of 10^{43-44} erg s^{-1} and a modest $\delta = 10$). This is important because it has been proposed that (lower-power) TeV BL Lacs are significant contributors to the heating of the intergalactic medium (IGM; e.g., Broderick et al. 2012; Chang et al. 2012; Lamberts et al. 2015, but see also Sironi & Giannios 2014), where the high-energy gamma-rays (>100 GeV) produced by these jets pair-produce off the extragalactic background light, eventually depositing kinetic energy through plasma instabilities. Clearly, if this mechanism is important, the large-scale jets of powerful quasars may be a far more important source of >100 GeV photons than TeV BL Lacs, and possibly the dominant class of sources for blazar heating.

We have not applied an EBL correction to these spectra merely to illustrate the total intrinsic output. However, EBL absorption is very important at TeV energies, and would make direct observation of this TeV component difficult. Even assuming the most optimistic case of $\delta = 7.8$ for 3C 273, at redshift 0.158 the EBL absorption (Finke et al. 2010) is already high enough that it would take at least 100 hours of observations by the future CTA mission to detect the beamed IC/CMB component at TeV energies. Thus it is unlikely that

many anomalous X-ray jets will have a synchrotron origin for the X-rays directly confirmed via TeV observations, though if *Fermi* begins detecting the IC/CMB component, an upturn at the highest energies might be visible in a few cases. The remaining best direct observation is via polarization—either in the UV, for those that show the second component emerging there, or with future X-ray polarimeters. Finally, we note that as long as *Fermi* continues to operate, the low background at the highest energies should allow continually improving constraints on the δ factors of large-scale jets.

4. CONCLUSIONS

We have shown that the expected gamma-ray emission required if quasar jets produce X-rays via IC/CMB has been ruled out in two quasar jets, 3C 273 and PKS 0637-752, at a high significance level using *Fermi* upper limits. Examining the evidence, we favor a synchrotron origin for the X-rays of their large-scale jets. This considerably relaxes the power requirements for the jet away from the near and super-Eddington values. We have shown that the limits on the IC/CMB gamma-rays constrain the jets to have δ values of <7.8 for 3C 273 and <6.5 for PKS 0637-752 assuming equipartition. A very interesting outcome of the synchrotron explanation of the X-rays is the prediction that quasar jets may radiate far more at TeV energies than TeV BL Lacs. Future work remains to see if 3C 273 and PKS 0637-752 are outliers, or if IC/CMB can be ruled out as the source of the anomalous X-rays for more quasar jets.

E. T. M. acknowledges Fermi Grant NNX13AO88G.

Facilities: Fermi, *HST* (ACS, NICMOS, WFPC2), CXO (ASIS), *Spitzer*, ATCA.

REFERENCES

Aharonian, F. A. 2002, MNRAS, 332, 215
Arshakian, T. G., & Longair, M. S. 2004, MNRAS, 351, 727
Atoyan, A., & Dermer, C. D. 2004, ApJ, 613, 151
Broderick, A. E., Chang, P., & Pfrommer, C. 2012, ApJ, 752, 22
Cara, M., Perlman, E. S., Uchiyama, Y., et al. 2013, ApJ, 773, 186
Celotti, A., Ghisellini, G., & Chiaberge, M. 2001, MNRAS, 321, L1
Chang, P., Broderick, A. E., & Pfrommer, C. 2012, ApJ, 752, 23
Chartas, G., Worrall, D. M., Birkinshaw, M., et al. 2000, ApJ, 542, 655
Dermer, C. D., & Atoyan, A. 2004, ApJL, 611, L9
Edwards, P. G., Piner, B. G., Tingay, S. J., et al. 2006, PASJ, 58, 233
Finke, J. D., Razzaque, S., & Dermer, C. D. 2010, ApJ, 712, 238
Georganopoulos, M., & Kazanas, D. 2004, ApJL, 604, L81
Georganopoulos, M., Perlman, E. S., Kazanas, D., & McEnery, J. 2006, ApJL, 653, L5
Ghisellini, G., & Tavecchio, F. 2010, MNRAS, 409, L79
Godfrey, L. E. H., Bicknell, G. V., Lovell, J. E. J., et al. 2012a, ApJ, 755, 174
Godfrey, L. E. H., Lovell, J. E. J., Burke-Spolaor, S., et al. 2012b, ApJL, 758, L27
Hardcastle, M. J. 2006, MNRAS, 366, 1465
Harris, D. E., & Krawczynski, H. 2006, ARA&A, 44, 463
Harris, D. E., Mossman, A. E., & Walker, R. C. 2004, ApJ, 615, 161
Jester, S., Röser, H.-J., Meisenheimer, K., & Perley, R. 2005, A&A, 431, 477
Jester, S., Röser, H.-J., Meisenheimer, K., & Perley, R. 2006, ApJ, 648, 900
Jorstad, S. G., Marscher, A. P., Lister, M. L., et al. 2005, AJ, 130, 1418
Kataoka, J., & Stawarz, Ł. 2005, ApJ, 622, 797
Kharb, P., Lister, M. L., Marshall, H. L., & Hogan, B. S. 2012, ApJ, 748, 81
Kundu, E., & Gupta, N. 2014, MNRAS, 444, L16
Lamberts, A., Chang, P., Pfrommer, C., et al. 2015, arXiv:1502.07980
Lister, M. L., Aller, M. F., Aller, H. D., et al. 2013, AJ, 146, 120
Lister, M. L., Cohen, M. H., Homan, D. C., et al. 2009, AJ, 138, 1874
Marshall, H. L., Gelbord, J. M., Schwartz, D. A., et al. 2011, ApJS, 193, 15
Marshall, H. L., Schwartz, D. A., Lovell, J. E. J., et al. 2005, ApJS, 156, 13
Mehta, K. T., Georganopoulos, M., Perlman, E. S., Padgett, C. A., & Chartas, G. 2009, ApJ, 690, 1706
Meyer, E. T., & Georganopoulos, M. 2014, ApJL, 780, L27
Mullin, L. M., & Hardcastle, M. J. 2009, MNRAS, 398, 1989
Nolan, P. L., Abdo, A. A., Ackermann, M., et al. 2012, ApJS, 199, 31
Sambruna, R. M., Gambill, J. K., Maraschi, L., et al. 2004, ApJ, 608, 698
Sambruna, R. M., Maraschi, L., Tavecchio, F., et al. 2002, ApJ, 571, 206
Sambruna, R. M., Urry, C. M., Tavecchio, F., et al. 2001, ApJL, 549, L161
Schwartz, D. A., Marshall, H. L., Lovell, J. E. J., et al. 2000, ApJL, 540, L69
Siemiginowska, A., Smith, R. K., Aldcroft, T. L., et al. 2003, ApJL, 598, L15
Siemiginowska, A., Stawarz, Ł., Cheung, C. C., et al. 2007, ApJ, 657, 145
Sironi, L., & Giannios, D. 2014, ApJ, 787, 49
Tavecchio, F., Maraschi, L., Sambruna, R. M., & Urry, C. M. 2000, ApJL, 544, L23
Uchiyama, Y., Urry, C. M., Cheung, C. C., et al. 2006, ApJ, 648, 910
Uchiyama, Y., Urry, C. M., van Duyne, J., et al. 2005, ApJL, 631, L113
Wilson, A. S., & Yang, Y. 2002, ApJ, 568, 133
Zhang, H., & Böttcher, M. 2013, ApJ, 774, 18